A bionic stem-shaped copper-doped aniline-pyrrole copolymer composite photothermal sponge evaporator for seawater desalination and sewage treatment

Yongjie Lao [a], Yusheng Wang [a], Qiao Zhang* [a], Feipeng Du [a], ChakYin Tang [b], ChiPong Tsui [b], Yunfei Zhang* [a]

[a] School of Materials Science and Engineering, Wuhan Institute of Technology, Wuhan 430205, China

[b] Department of Industrial and Systems Engineering. The Hong Kong Polytechnic University, Hung Hom, Hong Kong, People's Republic of China

*Corresponding Author (s): booyou@163.com (Q. Zhang); zyf3006@126.com (Y. Zhang)

Calculation of the evaporation rate and the efficiency

The evaporation rate ($\dot{m}$) and energy conversion efficiency (η) are calculated using equations (1-4) as detailed below [1, 2]:

$$\dot{m} = \frac{m}{At} \quad (1)$$

$$U_{in} = \Delta H_{vap} m_0 = \Delta H_{equ} m_g \quad (2)$$

$$h_{lv} = \lambda_{lv} + C_p(T_1 - T_0) \quad (3)$$

$$\eta = \frac{\dot{m} h_{lv}}{q} \times 100\% \quad (4)$$

In formula (1-4): m represents the water mass loss (g) in the evaporator; A represents the area of light that the evaporator is exposed to (m^{-2}); t represents the duration of evaporation (h); m is the evaporation rate (kg m^{-2} h^{-1}). ΔH_{vap} represents the enthalpy of evaporation of pure water at 2257 J g^{-1}, and m_0 represents the dark evaporation of pure water. ΔH_{equ} is the equivalent enthalpy of evaporation (J g^{-1}) of water in the evaporator, and m_g is the dark evaporation of water in the evaporator. U_{in} is an energy input from the outside. λ_{lv} is latent heat [equivalent to the equivalent enthalpy of evaporation ΔH_{equ} in (2)]; $C_p(T_1 - T_0)$ is the sensible heat in the evaporation system, where C_p is the specific heat capacity of water, T_1 is the steady-state temperature of the material, T_0 is the initial temperature of the material, and

h_{lv} is the enthalpy of phase transition in evaporation (J g^{-1}). η represents the evaporation efficiency of water bodies; q is the simulated solar intensity of vertical irradiation (kW m^{-2}). The evaporation rates of each sample shown in **Table S1** are calculated using formula (1)

Table S1 The evaporation rates of the prepared photothermal sponges

Photothermal sponges	Evaporation rate (kg m^{-2} h^{-1})
PVA	0.75
PANI/PVA	2.04
PPy/PVA	2.28
PANI-PPy/PVA-1	2.45
PANI-PPy/PVA-2	2.53
PANI-PPy/PVA-3	2.58
PANI-PPy/PVA-4	2.18
PANI-PPy/PVA-5	2.56
PANI-PPy/PVA-6	2.60
CuNPs@ PANI-PPy/PVA-1	3.01
CuNPs@ PANI-PPy/PVA-2	3.24
CuNPs@ PANI-PPy/PVA-3	3.25
CuNPs@ PANI-PPy/PVA-4	3.84
CuNPs@ PANI-PPy/PVA-5	3.35

Physical properties of CuNPs@PANI-PPy/PVA-4

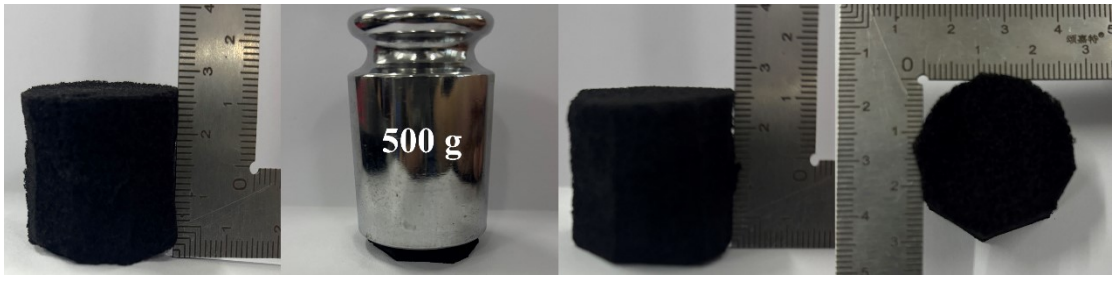

Fig. S1 Compression and recovery of the CuNPs@PANI-PPy/PVA-4.

As shown in **Fig. S1**, the prepared CuNPs@PANI-PPy/PVA-4 is a dark green cylinder. Before compression, the height of the sponge is approximately 27 mm. After loading a 500 g

weight, the sponge is significantly deformed. The CuNPs@PANI-PPy/PVA-4 sponge almost recovers the shape and height after unloading the weight, indicating the CuNPs@PANI-PPy/PVA-4 has good compression deformation and recovery performance.

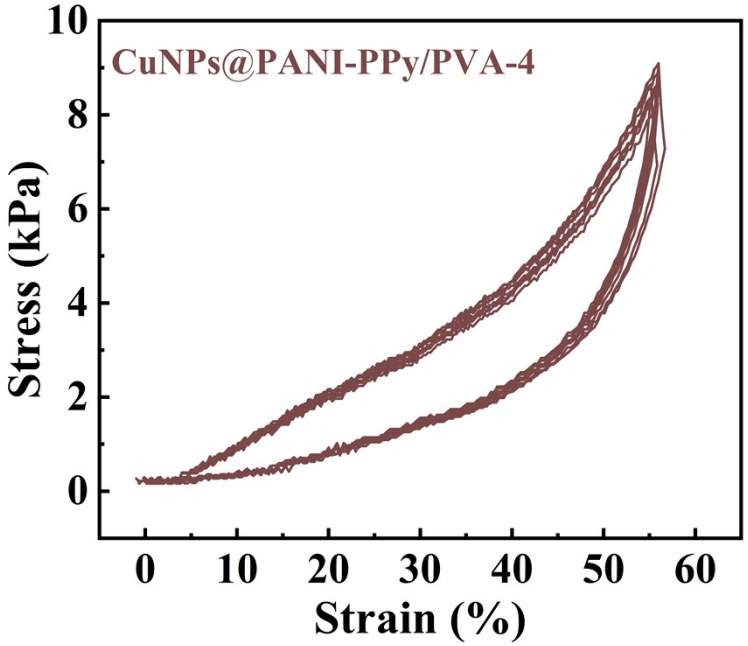

Fig. S2 10 cycles compression recovery test of CuNPs@PANI-PPy/PVA-4 at 55% strain.

Furthermore, 10 cycles of compression recovery test of CuNPs@PANI-PPy/PVA-4 are conducted at 55% strain. As shown in **Fig. S2**, the stress-strain curves of the samples during the cycling compression recovery test fit well together, demonstrating excellent compression recovery properties. Therefore, the CuNPs@PANI-PPy/PVA-4 sponge prepared has loose structure and low density characteristics.

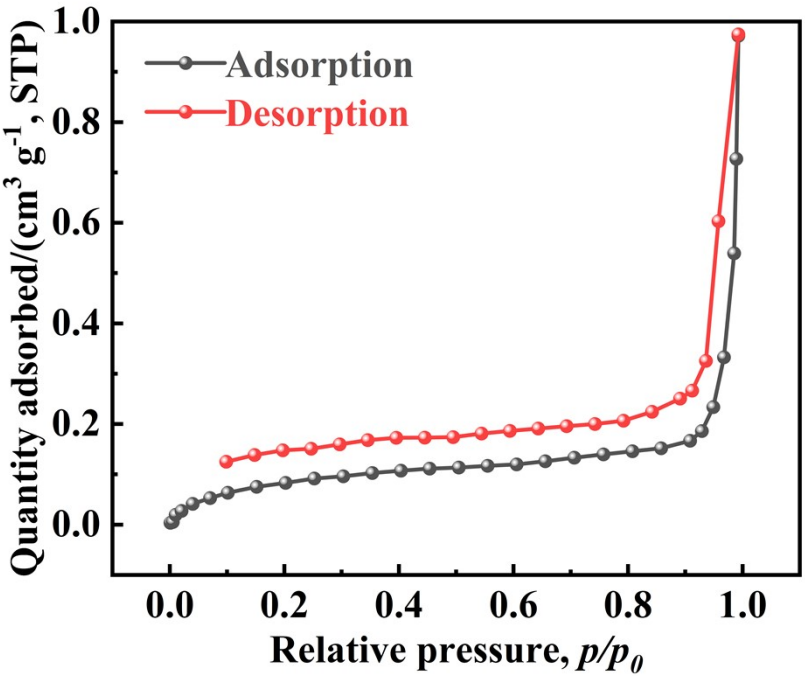

Fig. S3 Nitrogen adsorption desorption isotherms of CuNPs@PANI-PPy/PVA-4.

Nitrogen desorption and adsorption test is conducted to characterize the porous structure of CuNPs@PANI-PPy/PVA-4. In **Fig. S3**, the sponge demonstrates a type IV isothermal adsorption curve, and its adsorption-desorption isotherms do not overlap, forming H1 type hysteresis loop. The average pore size of the sponge is about 9.43 nm calculated by Barrett-Joyner-Halenda (BJH) method. Therefore, the prepared sponge shows a mesoporous structure. In addition, the specific surface area is about 1.68 m^{-2} g^{-1} calculated by BET method. The saturated adsorption platform existing in the curve reflects that the pore size of CuNPs@PANI-PPy/PVA-4 is relatively uniform, which is conducive to water transport and guarantee insufficient water supply during evaporation.

Seawater desalination test

As shown in **Fig. S4**, the purification effect of the simulated brine was evaluated by testing the resistance of the purified water with a digital multimeter. The resistance of the water collected by CuNPs@PANI-PPy/PVA-4 photothermal evaporation experiment was 135.88 kΩ, which was more than two orders of magnitude greater than the initially simulated real seawater (2.15 kΩ), and exceeded the normal value of the drinking water (30.47 kΩ). Therefore, the CuNPs@PANI-PPy/PVA-4 demonstrates good seawater desalination effect.

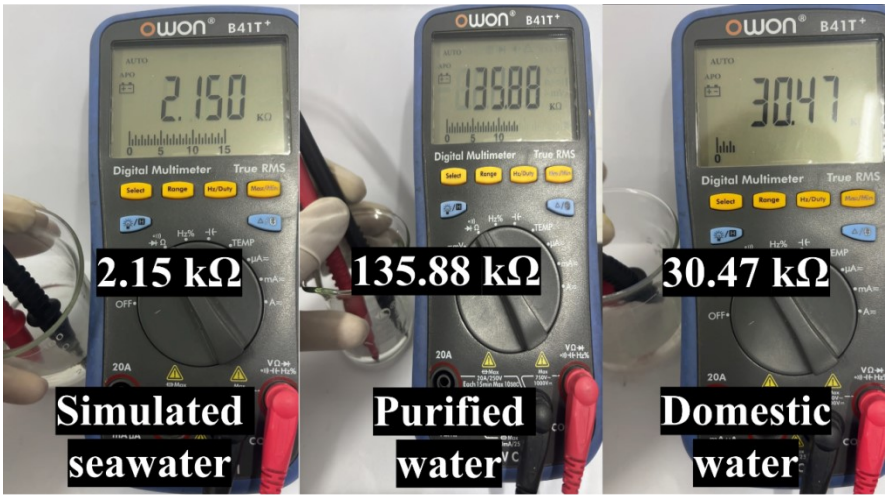

Fig. S4 The resistance of various water samples tested by a digital tester

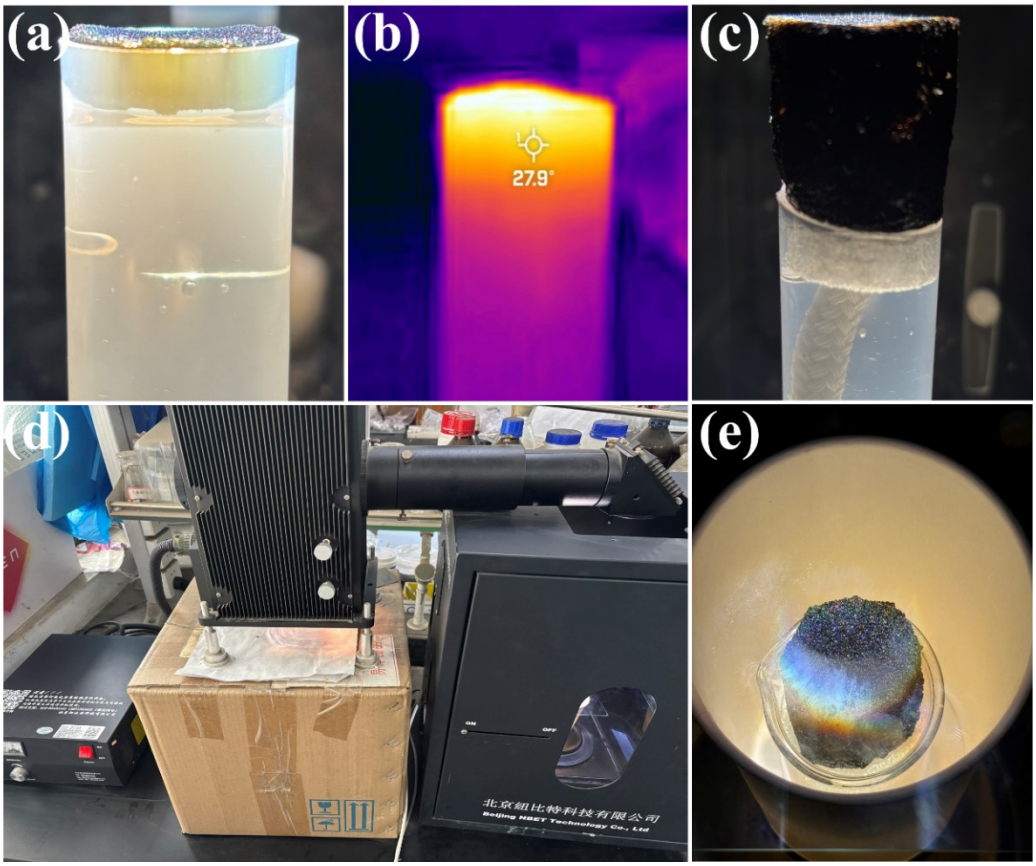

Fig. S5 (a) Digital photo of the traditional floating solar evaporation device, (b) traditional floating solar evaporation device infrared digital photograph, (c) digital photo of a biomimetic stem-shaped solar evaporation device, (d) digital photo of the solar xenon lamp simulator, (e) photo of indoor water collection and purification device

As shown in **Figs. S5(a, b)**, the traditional floating solar evaporation system directly contacts the water surface, resulting in significant heat loss to the underlying water body during the evaporation process. As shown in **Fig. S5(c)**, the biomimetic stem-shaped solar

evaporation device has a piece of polystyrene foam between the bottom of the CuNPs@PANI-PPy/PVA-4 and the water source below, which can effectively isolate the heat in the CuNPs@PANI-PPy/PVA-4 from the water below. As the solar evaporation process progresses, the cotton strips at the bottom of the CuNPs@PANI-PPy/PVA-4 can continuously supply water to the CuNPs@PANI-PPy/PVA-4, ensuring that the CuNPs@PANI-PPy/PVA-4 has sufficient water supply during the evaporation process. As shown in **Fig. S5(d)**, it is the solar xenon lamp simulator. As shown in **Fig. S5(e)**, CuNPs@PANI-PPy/PVA-4 was used for a simulated seawater desalination test in an indoor environment, and the process of collecting the purified water was carried out.

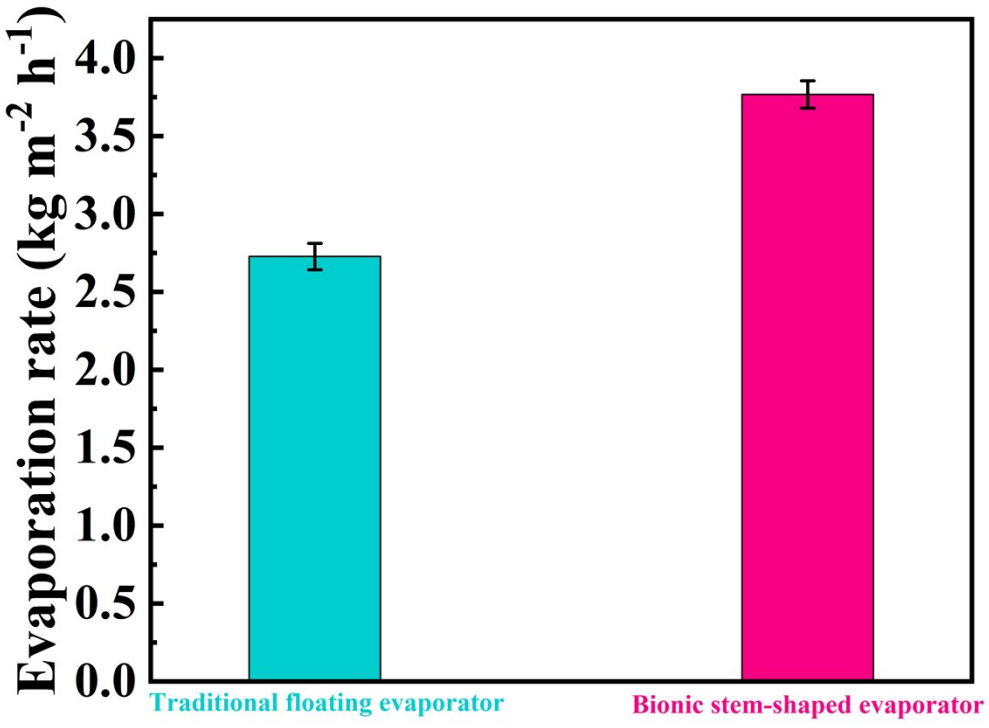

Fig. S6 Comparison chart of evaporation rates of the CuNPs@PANI-PPy/PVA-4 under two structural designs.

As shown in **Fig. S6**, the evaporation rate of the biomimetic stem-shaped evaporator is superior to that of the traditional floating evaporator.

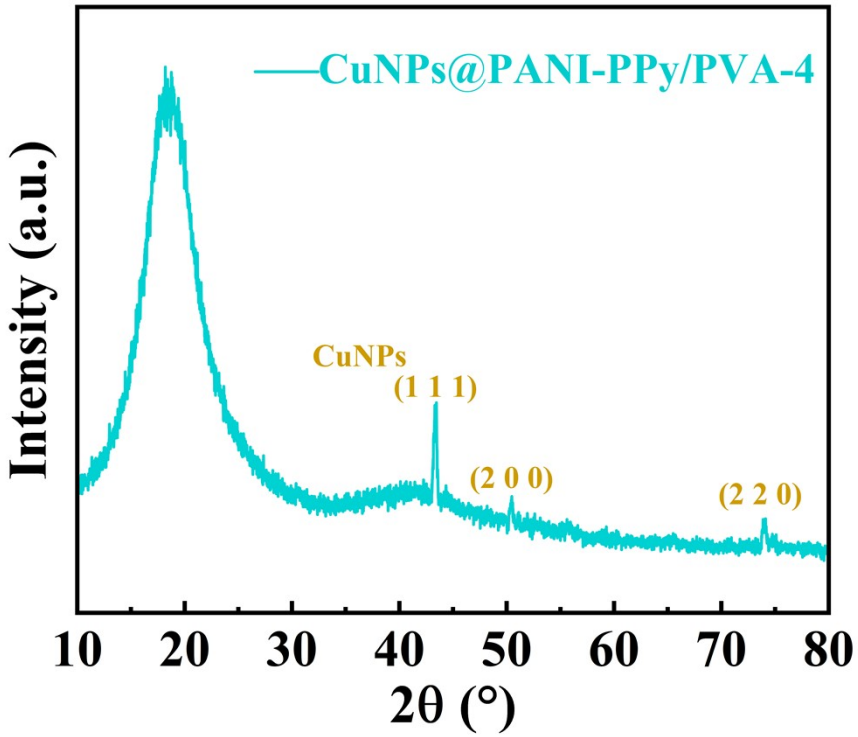

Fig. S7 XRD spectra of the CuNPs@PANI-PPy/PVA-4 after the cyclic simulated seawater experiment

In order to determine the long-term stability of copper nanoparticles under high salinity and repeated evaporation conditions, we conducted XRD tests on the CuNPs@PANI-PPy/PVA-4 after the cyclic simulation of seawater evaporation experiments. As shown in the **Fig. S7**, the peaks of nano-copper still exist, indicating that it has certain long-term stability.

The PVA sponge has a porous structure, and the pores of the sponge enable the reverse diffusion of salt through capillary action. As shown in **Fig. S8**, upon evaporation of water in the upper sponge layer, salt residues remain in the pores; however, capillary action draws seawater upward to re-dissolve the salt. Driven by the concentration gradient, high-salinity seawater diffuses toward low-salinity regions, maintaining system salt balance. Subsequent continuous evaporation sustains this cyclic dynamic equilibrium, preventing significant salt accumulation in the sponge that would otherwise impair evaporation efficiency.

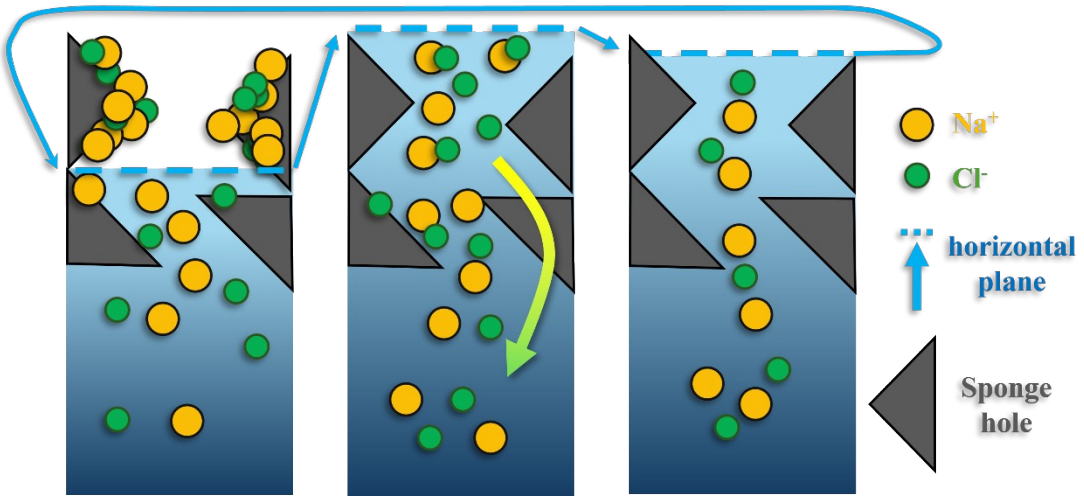

Fig. S8 Schematic of the Salt Back-Diffusion Mechanism

Table S2 Concentration of Cu^{2+} in purified water measured by ICP-MS.

Ions	Analogue seawater (mg L^{-1})	Acid-base wastewater (mg L^{-1})	Evaporated water (mg L^{-1})
Cu^{2+}	--	--	--

Table S3 Detailed information about the outdoor simulation experiment of solar evaporation

Time	Solar flux (kW m^{-2})	Temperature (°C)
11:00	907.7	19.1
12:00	844.8	20.3
13:00	901.7	21.2
14:00	897.4	21.6
15:00	662.8	21.1
16:00	33.0	19.8

References

1 X. Li, G. Ni, T. Cooper, N. Xu, J. Li, L. Zhou, X. Hu, B. Zhu, P. Yao and J. Zhu, *Joule*, 2019, **3**, 1798–1803.

2 T.A. Cooper, S.H. Zandavi, G.W. Ni, Y. Tsurimaki, Y. Huang, S.V. Boriskina and G. Chen,

1 Contactless steam generation and superheating under one sun illumination, *Nat. Commun.*,
2 2018, **9**, 5086.